

Power dependence of the electron mobility profile in a Hall thruster

Benjamin A. Jorns* Richard H. Hofer† and Ioannis G. Mikellides ‡

Jet Propulsion Laboratory, California Institute of Technology, Pasadena, CA 91109

The electron mobility profile is estimated in a 4.5 kW commercial Hall thruster as a function of discharge power. Internal measurements of plasma potential and electron temperature are made in the thruster channel with a high-speed translating probe. These measurements are presented for a range of throttling conditions from 150 - 400 V and 0.6 - 4.5 kW. The fluid-based solver, Hall2De, is used in conjunction with these internal plasma parameters to estimate the anomalous collision frequency profile at fixed voltage, 300 V, and three power levels. It is found that the anomalous collision frequency profile does not change significantly upstream of the location of the magnetic field peak but that the extent and magnitude of the anomalous collision frequency downstream of the magnetic peak does change with thruster power. These results are discussed in the context of developing phenomenological models for how the collision frequency profile depends on thruster operating conditions.

I. Introduction

The increased propellant efficiency and large Δv budgets of solar electric propulsion (SEP) make it a key enabler for several of the missions identified by the most recent Planetary Decadal Survey. However, the cost of government-built SEP systems¹⁻³ can be prohibitive given the current once-per-decade flight rate of SEP on NASA missions. Commercial systems represent a potential solution to this problem. With their higher flight rate, they can offer as much as 50% savings in production and qualification costs over government-developed systems.⁴ For example, Aerojet Rocketdyne's BPT-4000, a 4.5 kW class Hall thruster, is a flight-qualified commercial system that has been identified as a leading commercial candidate for deep space missions.⁴⁻⁷ It has a wide throttling range in both power and specific impulse, and its "magnetically-shielded" (MS) properties that onset after several thousands of hours of operation^{8,9} can accommodate the large propellant throughput required for long-range, deep space missions. The BPT-4000 also has demonstrated flight performance, having been flown successfully on the Air Force's Advanced EHF satellites, where it is employed for geosynchronous earth orbit applications.¹⁰

In light of this flight heritage and the studies that have demonstrated the throttling capability of the BPT-4000, the NASA Jet Propulsion Laboratory (JPL) is qualifying the BPT-4000 to a TRL 8 for deep-space missions. One of the major difficulties for achieving this end is that the timescales of deep space missions can exceed 10000s of hours. Lifetime qualifying the thruster through endurance testing therefore can be extremely costly and schedule limiting. Moreover, the throttling curves required for future missions are not yet known, which makes it impractical to test the thruster for a mission by directly recreating the required thrusting profile. A predictive model for thruster performance that is valid over arbitrary throttle curves would help resolve this difficulty for thruster qualification. However, even though there are high-fidelity Hall thruster models, these simulations are not fully predictive. This is a problem common to most Hall thruster models and stems from the fact that the mechanism for electron transport is anomalous and not well-understood.¹¹⁻¹⁸ In order to accurately simulate performance, it is necessary to specify the shape and magnitude of the electron mobility in the thruster. Since this is not known *a priori*, the correct profile can only be arrived at by iterating on possible solutions in the code and attempting to match the simulation to

*Associate Engineer, Electric Propulsion Group, AIAA Member, benjamin.a.jorns@jpl.nasa.gov

†Senior Engineer, Electric Propulsion Group, AIAA Associate Fellow

‡Principal Engineer, Electric Propulsion Group, AIAA Associate Fellow

measured plasma parameters and thruster performance. Hall thruster models therefore must be informed by experiment, and we find ourselves facing a similar problem that would be encountered for qualifying the thruster through lifetime testing: it is necessary to validate the model experimentally at each stage of life and throttling condition that may be encountered.

If the operating conditions do not change drastically, however, it has been shown that the same mobility profile can be used to achieve approximately correct predictions of performance.¹⁹ This suggests a path forward for how we might make predictions for arbitrary throttling curves. In particular, we can select discrete throttling points, experimentally characterize the thruster at these conditions, and use these results to determine the appropriate mobility profile in the code. We then can interpolate between these measured profiles in order to find one that is applicable for the desired operating condition. Provided we examine enough points over discharge voltage and thrust levels, we should be able to predict accurately what the appropriate mobility profile should be at intermediate values. The goal of this paper is to present the technique we have adopted for achieving this end and the initial results we have for how the measured mobility profile in the BPT-4000 changes as a function of power. In the first section, we describe the thruster, reported values for its performance, and the diagnostics we employed to measure its internal plasma parameters. In the second section, we present our measurements of plasma potential and temperature inside the thruster channel as a function of operating condition. In the third section, we use Hall2De,²⁰ JPL’s in-house fluid-based model, to determine the electron mobility profiles that most closely reproduce our internal measurements. In the fourth and final section, we discuss the implications of this work and how they pertain to on-going efforts to qualify the BPT-4000 for deep space missions.

II. Experimental Setup

A. Thruster

The BPT-4000 was developed through a joint effort between Lockheed Martin Space Systems and Aerojet Rocketdyne as a 4.5 kW electric propulsion system for GEO satellite applications.^{8,21,22} The qualification life test (QLT) for GEO applications of this system was completed in 2005,^{21,23} and a series of thrusters subsequently were flown on the Advanced EHF spacecraft for GEO orbit raising and station keeping purposes.¹⁰ Following the QLT in 2005, extended operation at low-power (1-2 kW) was demonstrated through a NASA-funded qualification life test extension (QLT-E). Aerojet Rocketdyne also has measured sub-kW performance and plume properties down to discharge powers of 0.3 kW.²² The QLT conducted at Aerojet revealed that between 5600 and 10400 h of operation, the thruster had reached a near steady-state erosion configuration. Physics-based modeling of the BPT-4000 subsequently identified this state as “magnetically shielded”^{8,9} capable of achieving throughput well in excess of 1000 kg. This property coupled with the throttling range of the thruster are two features that make the BPT-4000 an attractive candidate for cost-capped science missions such as the NASA Discovery and New Frontiers missions.

Discharge Voltage	Power (kW)	Thrust (mN)	Total I_{sp} (s)	Total Efficiency (%)
150	0.3	23.2	687	25.7
200	0.4	27.5	894	29.9
200	1.0	79.4	1143	44.2
300	0.6	36.0	1470	35.0
300	1.0	67.6	1391	45.1
300	1.5	99.0	1470	47.0
300	3.0	193.1	1728	54.0
300	4.5	280.4	1843	55.3
400	2.0	119.8	1781	52.0
400	3.0	280.4	1843	55.3
400	4.5	256.9	2035	56.3

Table 1: Table with operating conditions experimentally characterized during this investigation. Values are taken from Ref. 6.

For the tests performed here, we examined the operation of the thruster over several operating conditions that may be encountered for Discovery class missions but that also can be produced with the PPU already qualified for the BPT-4000. We used the Engineering Model 1 (EM1) of the thruster with rings that had been machined to the magnetically-shielded state found during the QLT. A similar model, the EM2, was the subject of a previous study performed at JPL⁶ where the performance over a range of throttling conditions was examined. The results of this study for the EM2 at the magnetically-shielded ring state are shown in Table 1. We draw particular attention to the four “corner” conditions for operation that were the main focus of the QLT in 2005, the 3 and 4.5 kW operating powers at 300 and 400 V.

B. Facility

Experiments were performed in the Owens Chamber at JPL. This 3 m diameter by 10 m long vacuum chamber has been used previously to test Hall and ion thrusters at power levels up to 20 kW. The facility is cryogenically pumped and is lined with graphite panels to minimize backspattered material to thruster surfaces. Base pressures of 10^{-7} torr are routinely achieved. Recent upgrades to the facility have increased the pumping speed to approximately 200 kl/s. At the maximum anode flow rate of 14.1 mg/s xenon we investigated in this study, the background pressure was 1.23×10^{-5} torr.

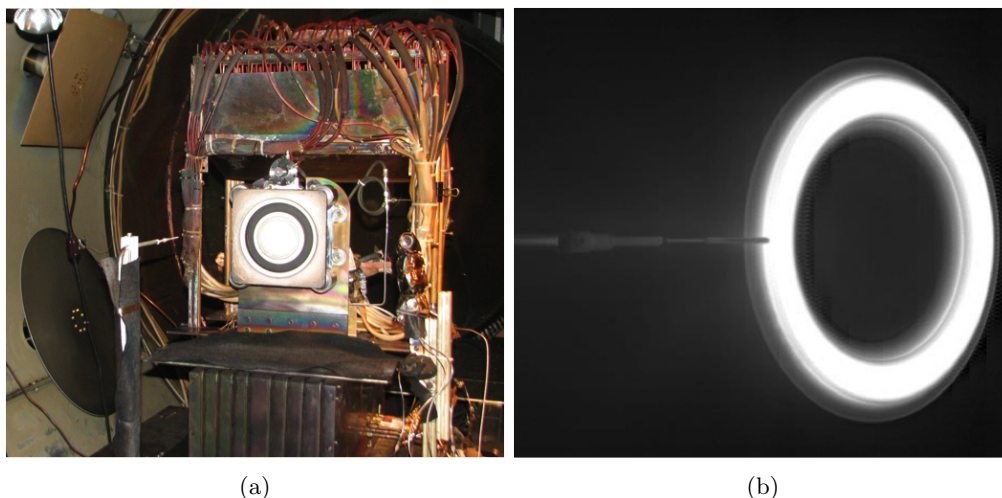


Figure 1: a) EM model of BPT-4000 installed in the Owens chamber at JPL. The probe arm is located in the foreground and mounted on a two-stage translation system. b) High speed image of probe as it crosses the exit plane during a shooting scan.

C. Power electronics and propellant delivery system

Power and propellant were delivered to the BPT-4000 with commercially available power supplies and flow controllers. The plasma discharge was sustained by a pair of power supplies wired in parallel capable of 500 V, 20 A operation. The discharge filter consisted of a $80 \mu\text{F}$ capacitor in parallel with the discharge power supply outputs. Additional power supplies were used to power the magnet coils and the cathode heater and keeper. The cathode heater and keeper were used only during the thruster ignition sequence. Research-grade xenon (99.9995% pure) was supplied through stainless steel feed lines with 50 and 500 sccm mass flow controllers. The controllers were calibrated before the experiment and were digitally controlled with an accuracy of 1% of the set point.

D. High-speed probes

We employed a high-speed translating probe for our internal measurements of the BPT-4000 as this system is less perturbative than a fixed probe array. In this setup, shown in Fig. 1a, the probe—Langmuir or emissive depending on measurement type—was mounted on a two-axis translation stage, which was capable of high-speed injection in the axial direction (see Ref. 24 for a full description of the stages). For each scan,

the probe was moved to a fixed radial position and a starting point axially downstream of the exit plane. We then shot the probe at high speed into the thruster channel. Fig. 1b shows an image of the probe as it crossed the thruster exit plane during thruster operation. For each shot, the probe was accelerated from the starting position, reached a maximum speed of 90 cm/s, and then decelerated to a stop 2-3 mm from the anode. It then was immediately retracted from the channel. The total length of the shots was typically < 0.1 s, and we monitored the position of the probe throughout the scan with string potentiometers.

During testing, the probe visually perturbed the plasma upon injection into the channel. This observation coupled with previous work on the perturbative effect of high-speed probe insertion²⁵ has led us to only report here data taken as the probe entered the channel.

1. Langmuir probe

We employed a single, cylindrical Langmuir probe (LP) for our internal measurements of the electron temperature. The active element was tungsten, 1.5 mm in length with a diameter of 0.25 mm. While the body of the probe was alumina, in order to minimize the effects of secondary electron emission, the end of the probe was covered in a sleeve of boron nitride. The diameter of the entire assembly including the insulator that entered the thruster channel was 3 mm. For our high-speed shots into the thruster channel, we triggered our data acquisition off a fixed position in space, two channel lengths downstream of the anode. Since the probe velocity profile was highly repeatable, this triggering technique allowed us to average the measured spatial profiles over multiple shots into the channel. For example, during our electron temperature investigation, we first measured the spatial dependence of the floating potential as averaged over three shots into the channel (Fig. 2a). We then superimposed a ramp pattern of voltage sweeps on this average floating potential and used an arbitrary waveform generator coupled with a bi-operational amplifier to generate a voltage pattern that varied as the probe was shot into the channel (Fig. 2b). The form of this applied voltage permitted us to sweep through the ion saturation and plasma potential locally without driving the probe too far into electron saturation. An example for the recorded current from the applied sweeps is shown in Fig. 2c.

The potential that we superimposed on the floating potential was a single-sided ramp with a frequency of 300 Hz and a 75% duty cycle. We chose this relatively low sweep rate and shape in order to minimize capacitive effects that can be incurred by applying a continuous sinusoid to the probe tip at high speed. In order to extract electron temperature from the IV traces, we fit an exponential function with an offset²⁶ to the measured probe current in the vicinity of each trace's floating potential (see Fig. 2d). Since the probe was translating during the probe sweeps, each measurement had an inherent spatial uncertainty associated with it equal to the distance the probe traveled when the fitted data was taken (the highlighted portion of Fig. 2d). On average, this positional error was ~ 1 mm, though the resolution of the individual data points was lower than this since the 300 Hz sweep rate only yielded 30 IV traces per probe injection. For the data reported here, the electron temperatures represent the average from five axial injections.

2. Emissive probe

The emissive probe we employed for this experimental investigation consisted of two tubes of alumina housed in a double-bore sleeve of boron nitride. The active element was a tungsten loop, 0.127 mm in diameter, with a length from insulator to tip of 2 mm. The total width of the probe component entering the channel was 5 mm. For each shot into the channel, we first would draw current through the probe loop until it began to emit and then monitor the floating potential, referenced to cathode common, as the probe traversed the channel. We then incrementally increased the heating current to the probe between shots until the measured floating potential near the anode began to asymptote (Fig. 3b)—an indication that the potential at the probe tip was approaching the plasma potential at this point. Throughout this process, the probe typically would only last for 5 - 10 shots before sufficient material was ablated to electrically open the loop. This limited number of shots coupled with the time constraints of replacing the probe between trials precluded us from averaging over multiple shots or using the emissive probe to scan all the operating conditions examined here. In particular, we only report single-shot measurements on the channel centerline at the four corner conditions of 3 and 4.5 kW at 300 and 400 V.

Employing the thin-sheath approximation (c.f. Ref. 26) for our Langmuir probe measurements in the channel (described above), our estimates of plasma density and electron temperature suggested a ratio $\mathcal{O}(r_p/\lambda_{de}) \sim 1$, where λ_{de} is the plasma Debye length and r_p is the probe radius. Following the sheath model developed by Fruchtmann et al.²⁷ for a cylindrical space-charge limited, electron-emitting probe, it is

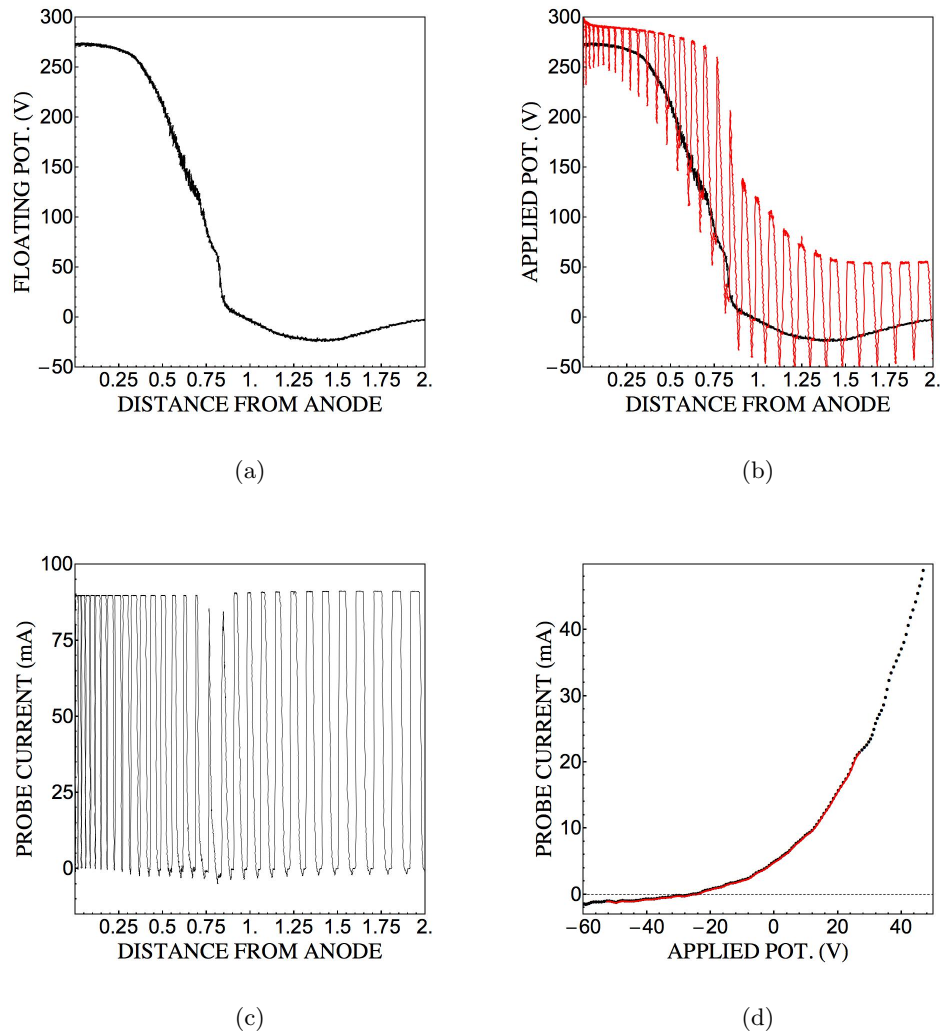


Figure 2: a) The floating potential measured on channel centerline as a function of distance from the anode. b) Voltage sweeps imposed on the floating potential as the probe is shot into the plasma. c) Resulting current measured by the probe. The saturation at 90 mA is due to the current limit of the power supply. d) Sample IV trace taken at position 1.25. The highlighted region corresponds to the data from which the electron temperature was extracted. The position has been normalized in all of these plots by the distance from the anode to the location of magnetic field peak. The operating condition shown is 300 V and 4.5 kW.

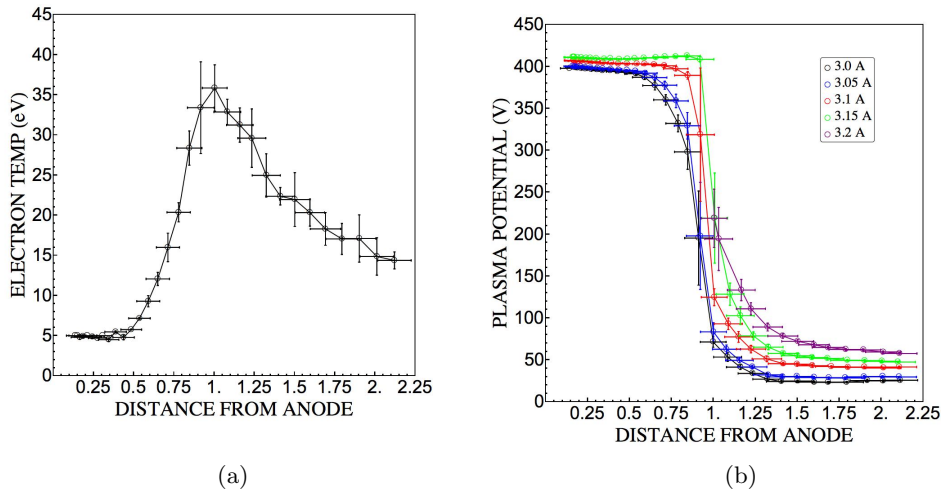


Figure 3: a) Measured spatial dependence of electron temperature at the operating condition 400 V and 4.5 kW. b) The spatial dependence of plasma potential as a function of increasing heater current drawn through the emissive probe. The voltage is referenced to cathode common, and a $0.5T_e$ correction has been applied from the data in (a).

necessary in this limit to add $0.5T_e$ to the measured potential in order to estimate the true plasma potential. This correction is valid provided the probe is space-charge limited; however, approaching this limit requires a sufficient level of probe heating. This level in turn is dependent both on the current applied to the probe loop as well as the self-heating from electron collection from the plasma. Since the electron temperature and plasma density vary significantly as a function of axial position, determining the right balance between applied heating and self-heating of the probe *a priori* is extremely difficult. Indeed, we have observed that we need to apply larger currents to the probe in the near plume than in the channel to approach the space charge limit. Using the probe current appropriate for the near plume, however, invariably led to the destruction of the probe inside the probe (see the 3.2 A case in Fig. 3). This made it nearly impossible to measure the total correct plasma profile with a fixed heater current. It may be possible to vary the imposed current on the probe in order to better capture the plasma profile, but we found that the thermal timescales for heating the probe with applied current were longer than the probe transit time, 0.1 s. In light of these difficulties, we ultimately concluded that our emissive probe measurements of potential provided qualitative trends at best.

III. Experimental Results

In the following section, we present the results of our experimental characterization of BPT-4000 EM1 at the throttling conditions specified in Table 1. We divide this data into three sections in order to illustrate the most relevant trends. In the first parts, we present centerline measurements at the four corner conditions that the BPT-4000 was primarily flight qualified for in the original QLT.²¹ In the second part, we present channel centerline measurements of electron temperature for several operating powers. In the third part, we show two dimensional contour maps of electron temperature for select operating conditions.

A. Centerline measurements at the four corner conditions

We show in Fig. 4 channel centerline measurements for the four corner operating conditions of the BPT-4000: 3 kW and 4.5 kW at 300 and 400 V. The peak in electron temperature in these figures is approximately coincident with the position of peak magnetic field. This is a physically intuitive result as the magnetic field impedes electron motion. The location of electric field (location of steepest gradient in plasma potential) also appears to follow this trend, though we note in the 300 V cases that the location of steepest gradient in potential is actually upstream of the electron temperature peak. This deviation may be a physically real result, but in light of the caveats for potential measurements we outlined in the previous section, it is also

possible that the emissive probe has not reached the space-charge limit. From these figures we can see from the data downstream of the magnetic field peak that the electron temperature scales with discharge voltage. This is consistent with the rule of thumb for power balance in Hall thruster discharges (c.f. Ref. 28).

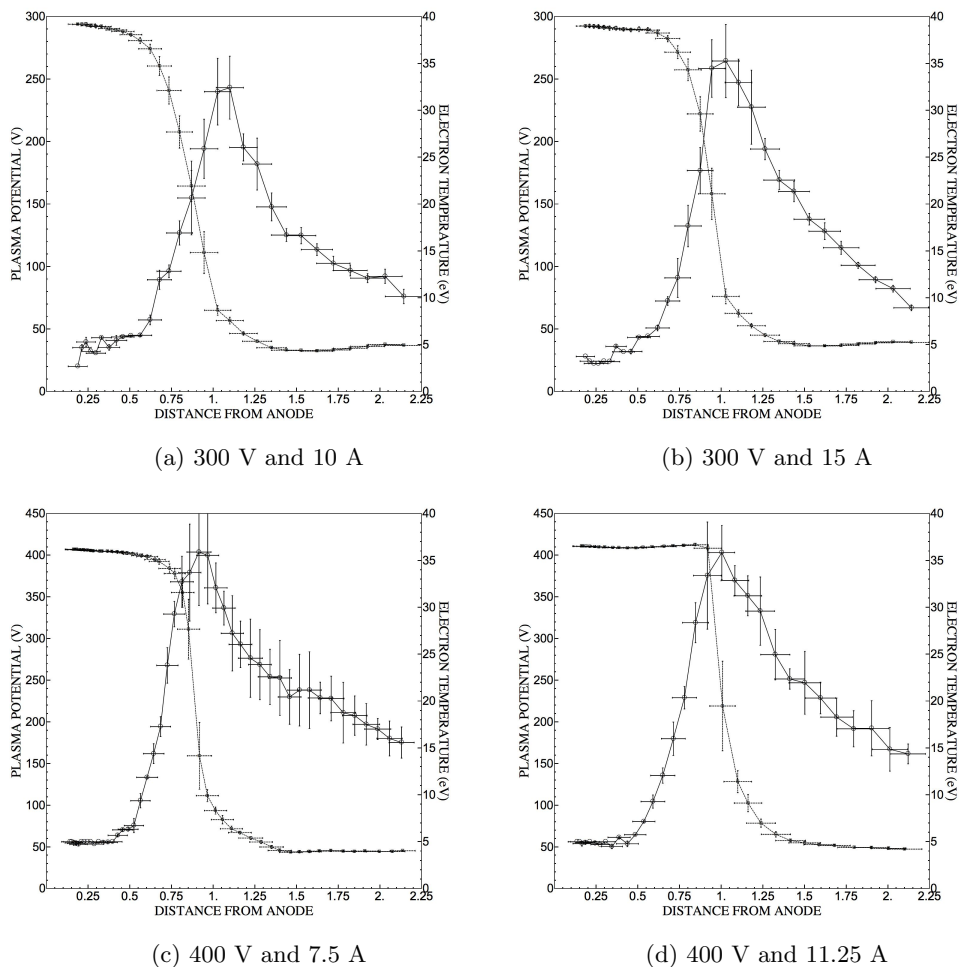


Figure 4: Measurements at channel centerline of electron temperature and plasma potential the four corner operating conditions of the BPT-4000. The position has been normalized by the distance from the anode to the location of peak magnetic field.

B. Centerline measurements as a function of thruster power

We show in Fig. 5 the electron temperature on centerline for varying power (as embodied by discharge voltage) at two conditions of fixed discharge current, $I_D = 2$ A and $I_D = 5$ A. From these plots, we can see that nearly the entire temperature profile scales with discharge voltage. This again is consistent with the understanding of the power balance in Hall thrusters where the electron temperature reflects the the energy in the discharge.²⁸ We also note that in the $I_D = 2$ A case, the location of the peak in electron temperature remains constant and near the location of peak magnetic field. For $I_D = 5$ A, on the other hand, the temperature peak for the 300 and 400 V cases is coincident with the location of the peak magnetic field but appears to shift upstream at 200 V.

In Fig. 6, we show the electron temperature on centerline for fixed voltage and varying power (as embodied by discharge current). From the 300 V case, we can see that within error bars the magnitude and location of the peak electron temperature as well as the shape of the electron temperature upstream of the peak magnetic field remain approximately the same. This is not the case for the temperatures downstream of the peak magnetic field. In particular for discharge currents at 5 A and above, temperatures downstream of the

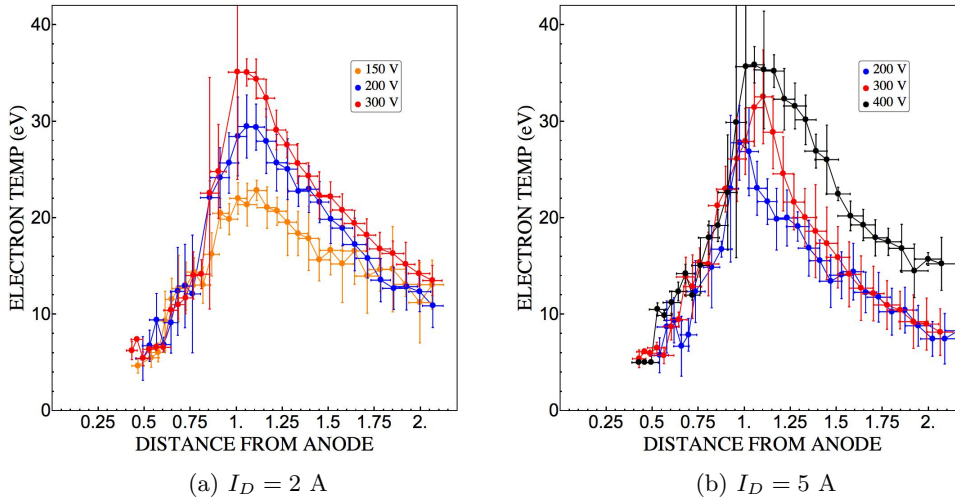


Figure 5: Measurements at channel centerline of the spatial dependence of electron temperature for fixed current and varying voltage.

peak temperature are inversely related with discharge current, which suggests that the temperature gradient (and therefore local heating) is more enhanced with increasing discharge current. The cases at 2 and 3.33 A for the 300 V case defy this trend, however, by having the largest electron temperatures downstream of the peak. For the 400 V case, the peak in electron temperature also appears to be located within error bars near the region of peak magnetic field. However, unlike the 300 V case, the shape of the electron temperature both upstream and downstream of this peak changes with discharge current. Since there are fewer conditions, it is difficult to isolate trends, though we note that the profile does appear to shift with discharge current—upstream when going from 5 A to 7.5 A but then downstream when moving from 7.5 A to 11.25 A.

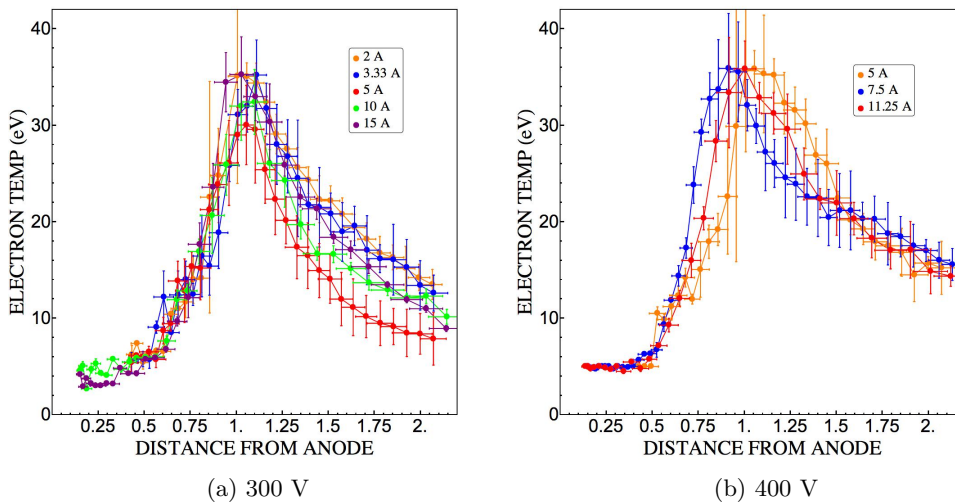


Figure 6: Measurements at channel centerline of the spatial dependence of electron temperature for fixed voltage and varying current.

C. Two-dimensional contour plots

In Fig. 7, we show two dimensional contour plots of the plasma electron temperature in the thruster channel. The axial coordinate in these figures has been normalized by the location of the peak in radial magnetic field, and the radial coordinate has been normalized by the channel width. These contours represent data

from five equally spaced radial shots into the thruster channel. It is significant to note that the peak electron temperature is still approximately coincident with the location of peak magnetic field and that it is located *downstream* of the thruster exit plane. This is an important observation since this region of peak temperature is also where the effects of anomalous resistivity begin to become dominant. Since it is downstream of the confining walls, this suggests that wall effects can largely be ignored in considering the dominant transport process in this thruster.

Upstream of the peak, we note that the temperature contours in all the plots appear to exhibit a characteristic concavity. This smooth bowing may indicate approximate isothermality of the magnetic field lines in this upstream region, though we note this same effect does not appear for electron temperature contours near the regions of peak magnetic field. Indeed, in an aberration that is particularly apparent for the 300 and 400 V, 4.5 kW cases and the 400 V, 3 kW case, we can see that the electron temperature contours at the peak magnetic field do not correspond to any possible magnetic field line in the thruster. Since there is strong experimental evidence that the magnetic field lines should be isothermal in the channel,²⁹ there is reason to believe that the deviation of our contours from isothermality may be artificially induced by probe perturbation. This effect has been shown to be important²⁵ but has not been fully elucidated to date.

Despite this possible source of error, however, our results do offer significant quantitative and qualitative insight into the internal character of the BPT-4000. In the next section we use these results to turn to the question of what internal processes, and in particular, what electron mobility profile, could lead to the observed experimental trends in electron temperature.

IV. Model for BPT-4000 operation

Hall2De is the model we will use to predict the throughput of the BPT-4000 for the throttling conditions of specific missions. This in-house code was developed at the Jet Propulsion Laboratory¹⁸ and is a 2D axisymmetric, magnetic field-aligned mesh, fluid solver. It is particularly apt for our problem since it has already been used to simulate and explain the long-life behavior of the BPT-4000.⁹ A number of upgrades recently have been implemented into this code including modifications to the ion-solver and improvements to its ability to incorporate multiple ion fluids that account for low energy ions born in the plume.³⁰ This latter feature provides increased fidelity at the thruster exit plane where low energy ions account for a significant fraction of the plasma density. For the simulations here, we take advantage of this upgrade by simulating the plasma as an electron fluid and two ion fluids, each with up to three possible charge states. The two fluids are differentiated by energy, where ions born at plasma potential above 50 V belong to the second fluid and those born at potential below 50 V belong to the second. We also note that the BPT-4000 cathode is externally mounted and therefore violates the axisymmetry inherent to Hall2De. The effect of this cathode therefore must be approximated as a plasma source spread uniformly in the azimuthal direction.

Hall2De is a fully predictive code with the exception that the spatial dependence of the anomalous collision frequency must be specified along the channel centerline. As with any Hall thruster code, without this anomalous collisionality, classical collisions are too weak for the simulation to accurately capture thrust, current, and experimentally-measured plasma parameters. The goal of this section is to attempt to arrive at forms for the anomalous collision frequency profile that yield plasma parameters consistent with our experimental measurements and operating parameters. Matching experimentally-measured parameters is an open-ended problem, however, given the wide variability of possible electron mobility profiles in the channel—Hall2De alone has twelve independent parameters for specifying the magnitude and spatial dependence of the profile. Ideally, the simulated solution should yield the same discharge current, thrust, and spatial dependence of plasma parameters as measured experimentally. However, there are three major caveats specific to the code that preclude the possibility of making an exact match between simulation and experiment. First, we found that our simulations consistently under predicted the reported values of thrust. Second, as we noted in Sec. II.D, the uncertainty as to the self-heating of the emissive probe renders measurements of plasma potential qualitative at best. And third, the fact that probes have been demonstrated to disturb the plasma once they pass the acceleration zone in the channel²⁵ suggests the temperature measurements at the peak and upstream of the magnetic field peak are also suspect.

We took all of these considerations into account when determining a method for finding the appropriate collision frequency profile. This led to the following guidelines:

- The discharge current must be matched by the simulation, I_D .

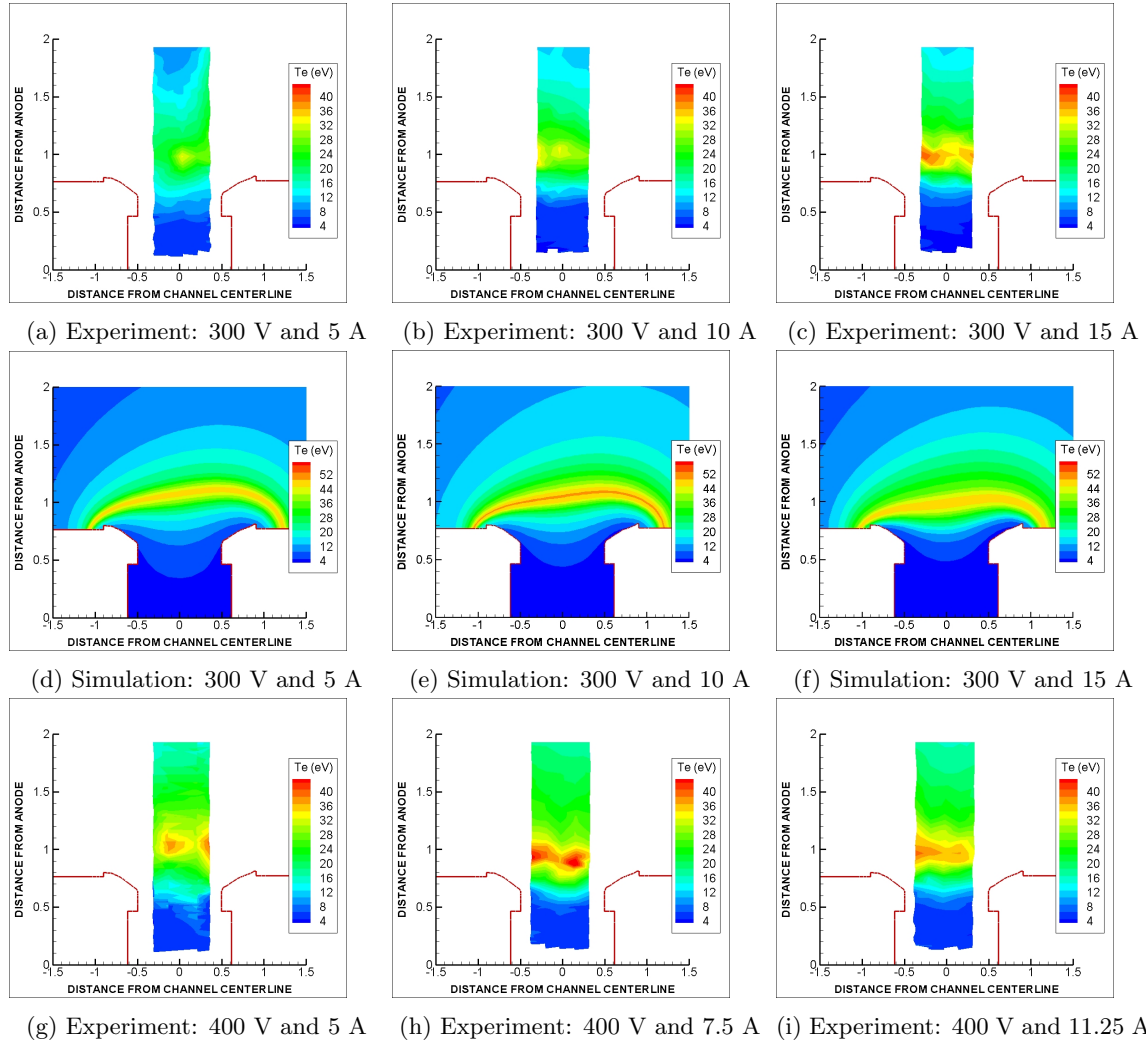


Figure 7: Experimental contour plots of electron temperature for increasing power at 300 V, (a)-(c), and 400 V, (g)-(i). The cases (d)-(f) show the results from simulations performed with Hall2De for the same 300 V operating conditions as (a)-(c). The axial coordinate in each plot has been normalized by the distance from the anode to the location of the peak radial magnetic field. The radial coordinate has been normalized by the channel width.

- The thrust of the simulation must be within 15%.
- The simulated electron temperature should match the measured temperature *downstream* of the electron temperature peak.

Following these guidelines, we iterated on the mobility profile to generate the electron temperature profiles at centerline for the three cases shown in Fig. 8: 1.5, 3, and 4.5 kW operating power at 300 V. We include the experimental data for comparison. From these plots, we can see that the downstream gradients in temperature are accurately captured by the simulation, but the peak in temperature at 45 eV is higher than that exhibited by the experimental data. This overestimate for electron temperature has been encountered before in Hall2De simulations of magnetically-shielded thrusters,²⁹ but the reason for it is not at present known. We show in Fig. 7d- 7f the comparison of the simulated data in two-dimensions with the internal measurements in Fig. 7a- 7c. There is qualitative agreement with the shape of the temperature contours exhibited by the simulations. However, since the magnetic field lines in Hall2De are stipulated to be isothermal,²⁰ the modeled results deviate from the non-isothermal temperature contours exhibited by the experimental results near the electron temperature peak.

The code-indicated performance parameters are listed in Table 2 along with the experimentally-measured results. As we indicated in the previous section, the discharge current is chosen to match the experimental current but the thrust is underestimated by the code. There is an exception at 5 A, where there is marked agreement between the predicted and measured thrust.

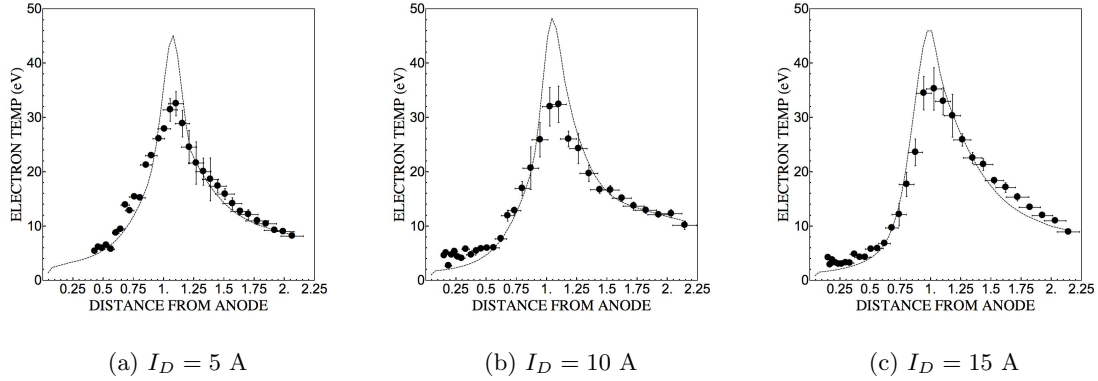


Figure 8: Comparison between simulated electron temperature with Hall2De (broken line) and experimental measurements at the channel centerline. The discharge voltage is 300 V for all three cases.

We show in Fig. 9a the three anomalous collision frequency profiles that yielded the results shown in Fig. 8. Each of these profiles shares common features with the others, which are consistent with the spatial dependence of collision frequency identified in previous work.¹⁷ In particular, there are three distinct dependencies of the collision frequency. The first, which occurs before the peak in magnetic field, is characterized by a low anomalous collision frequency. The classical collisions dominate in this region (Fig. 9b), and it therefore is unsurprising that the required collision frequency from the anomalous profile only changes by a factor of two as a function of power. The third region for collision frequency occurs downstream of the magnetic field peak and is Bohm-like, scaling inversely with magnetic field, $1/B$. The intermediate region between the first and third is a transitional one around the region of peak magnetic field where the anomalous collision becomes the dominant effect (Fig. 9b). The dip in the collision profile around $Z = 1$ corresponds to a region of low cross-field conductivity and therefore specifies the location of the peak electron temperature. The location of this dip does not change significantly as a function of discharge power, since the location of the peak electron temperature does not shift (Fig. 6a). Again, the magnitude of the dip in collision frequency only varies by a factor of two.

The most significant change among the different power cases shown in Fig. 9a occurs in the second and third regimes of collision frequency. In particular, the transition from the second regime to the third occurs at different points, $Z = 1.9, 1.7,$ and 2.1 for the $I_D = 5, 10,$ and 15 A cases respectively. The scaling factor for the Bohm like diffusion in the third region also shifts to a lower value for the $I_D = 5$ A case as compared to the $I_D = 10, 15$ A cases. The net effect of these shifts is that the slope of the collision frequency profile in the transition from the dip to the collision frequency peak is approximately the same for the $I_D = 5, 15$ A

Power (kW)	Exp. Thrust (mN)	Sim. Thrust (mN)	Exp. Total I_{sp} (s)	Sim. Anode I_{sp} (s)
1.5	99	94.5	1470	1497
3.0	193.1	167	1728	1656
4.5	280.4	259	1843	1875

Table 2: Table comparing predicted operating conditions with experimentally observed performance at the three simulated conditions. The discharge voltage is 300 V.

cases but has a smaller magnitude than that exhibited by the $I_D = 10$ A case. The reason for this non-monotonic dependence of the slope is not immediately clear. On one hand, enhanced collisionality allows for additional cross-field transport. This lowers the required electric field to generate cross-field current in the region downstream of the temperature peak, which suggests that the electron temperature should be lower for profiles where the transitional collision frequency is high. This trend is borne out by comparing the cases of $I_D = 15$ A and $I_D = 10$ A in Fig. 6a, but it is violated by the 5 A case. Its electron temperature in this transitional region is the lowest, but it has a lower collision frequency than the $I_D = 10$ A case. Another effect to consider is that since cross-field transport is facilitated by increasing collision frequency, the higher current cases should require enhanced collisionality in order to achieve the necessary current flow. This is evidenced by the fact that the 5 A case has the lowest collision frequency in the Bohm-like region as compared with the $I_D = 10, 15$ A cases. On the other hand, the 15 A case has a lower anomalous collision frequency than the 10 A in the transitional regime even though it supports a higher current.

The two effects of increased local joule heating and the need to accommodate higher current appear to have counteracting effects. This may in part explain the non-monotonic dependence of the collision frequency profile on discharge current; however, we note that these effects are also convolved with several other effects that change as a function of discharge current, e.g. density, ionization rates, and divergence. As we continue with this investigation and examine more measured conditions, we expect that more clear trends will emerge.

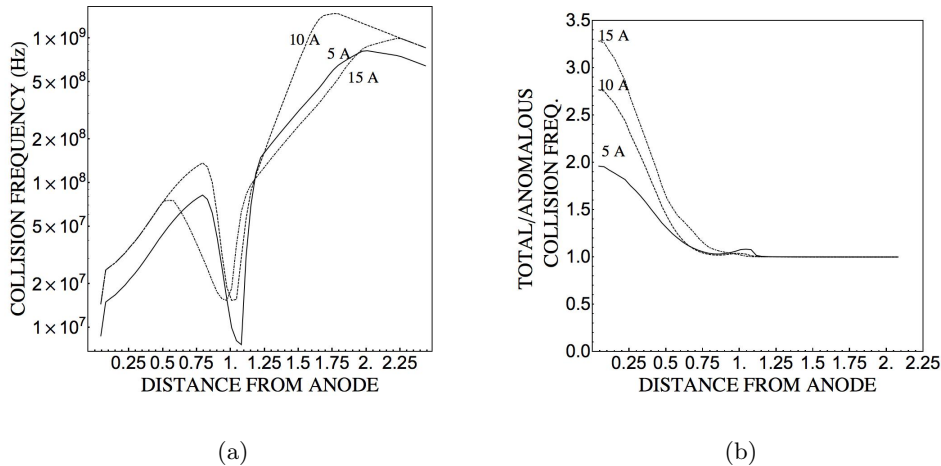


Figure 9: a) The anomalous collision frequency profiles at channel centerline that yielded the Hall2De results shown in Fig. 8. b) The Hall2De estimated ratio of anomalous collision frequency to the total electron collision frequency as a function of distance from the anode. The discharge voltage is 300 V for all three cases.

V. Discussion

This investigation has served three purposes. We have generated internal data on the BPT-4000 over a wide throttling range. We have determined guidelines of how to determine appropriate mobility profiles at these operating conditions with Hall2De. And we have started the process of identifying trends for the mobility profiles that may ultimately allow us to interpolate between measured conditions.

This last component will be particularly important as we move forward with our qualification efforts. In particular, from this investigation we have learned that the anomalous collision frequency upstream of the magnetic field peak does not change significantly with discharge power since it is dominated by classical effects. Similarly, we have found the location of the temperature peak is approximately fixed as a function of operating condition. This allows us to fix the position of the dip in the collision frequency profile for arbitrary operating condition. On the other hand, we have noted that the most significant parameters that changed for our three cases were the location and magnitude of the Bohm-like regime. This latter observation suggests that a strategy for interpolating between discrete operating points will rely on a more detailed analysis of the parts of the collision frequency profile downstream of the magnetic field peak. In particular, while it appears as if we can assume an average collision frequency profile for all points up to the location of the peak electron temperature, we will need to determine phenomenological scaling laws for how the Bohm-scaling factor and the location of the transition between the second and third regimes changes as a function of operating conditions. This is the subject of our ongoing investigation, which we will continue to pursue with the metrics we have outlined in this work. In parallel with these efforts, it will be necessary to resolve the discrepancy in thrust and electron temperature magnitude that are currently observed in Hall2De simulations of the BPT-4000.

Once we have simulated all of the operating conditions outlined above and established a means to interpolate between them, the next step will be to validate the predictive capability of the code. In particular, we will select operating points between our measured parameters and attempt to use the code to predict the performance. The simulations then will be checked with experimental measurements.

VI. Conclusion

In this paper we have presented the initial results of our effort to determine the electron mobility in the BPT-4000 for the throttling conditions that may be encountered in deep-space missions. We have presented experimental measurements for the electron temperature and plasma potential inside the thruster channel, and we have made note of the trends these parameters exhibit with operating conditions. In particular, we found, as would be expected from power balance models of the thruster, that the magnitude of the electron temperature scales with discharge voltage. We similarly noted that the peak in electron temperature is almost invariably coincident with the location of the peak radial magnetic field.

Through the use of Hall2De, JPL's in-house fluid-based code, we have modeled three operating conditions of the thruster at fixed voltage, 300 V, and increasing thruster power. We showed that changing the discharge current will shift the magnitude of the scaling factor for the Bohm-like collision frequency that occurs downstream of the peak magnetic field as well as the location where the transition to this Bohm-scaling occurs. We also found that changes in the mobility profile upstream of the magnetic field peak had only a small impact on modeling thruster characteristics. This was because classical collisions dominated in this region, and the experimentally determined location of the peak in electron temperature did not appear to shift with operating condition. Our observation that the critical parameters for the collision frequency profile occur downstream of the magnetic field peak suggests a path forward for interpolating between measured throttling conditions with Hall2De. In particular, as we continue with this research effort, we will attempt to generate phenomenological models for how the location and magnitude of the Bohm-like region changes as a function of operating conditions. The ultimate goal will be to develop a means to interpolate between measured conditions in such a way that we can predict thruster performance at operating conditions that have not been examined previously.

Acknowledgments

The research described in this paper was carried out by the Jet Propulsion Laboratory, California Institute of Technology, under a contract with the National Aeronautics and Space Administration and funded through the internal Research and Technology Development program. These experiments would not have been possible without the generous loan of the EM1 BPT-4000 that was provided by Aerojet Rocketdyne and Lockheed Martin. We would like to thank Vadim Khayms at Lockheed Martin for supporting the hardware loan and Alex Mathers at Aerojet Rocketdyne for preparing the thruster and providing support for the experiments throughout. We also would like to acknowledge the assistance of Dr. Alejandro Ortega, NASA JPL, with preparing the mesh for the Hall2De simulations.

References

- ¹Brophy, J. R., Garner, C. E., and Mikes, S. C., "Dawn Ion Propulsion System: Initial Checkout After Launch," *Journal of Propulsion and Power*, Vol. 25, No. 6, Nov. 2009, pp. 1189–1202.
- ²Garner, C. E., Rayman, M. D., and Brophy, J. R., "In - Flight Operation of the Dawn Ion Propulsion System Through Year One of Cruise to Ceres," *49th AIAA/ASME/SAE/ASEE Joint Propulsion Conference, July 14-17, San Jose, CA. AIAA-2013-4112*, 2013.
- ³Herman, D., Soulas, G. C., Van Noord, J. L., and Patterson, M. J., "NASA's Evolutionary Xenon Thruster (NEXT) Long-Duration Test Results," *Journal of Propulsion and Power*, Vol. 28, No. 3, May 2012, pp. 625–635.
- ⁴Hofer, R. R., Randolph, T. M., Oh, D. Y., Snyder, J. S., and De Grys, K., "Evaluation of a 4.5 kW Commercial Hall Thruster System for NASA Science Missions," *42nd AIAA/ASME/SEA/ASEE Joint Propulsion Conference, July 9-12, 2006, Sacramento, CA. AIAA-2006-4469*.
- ⁵Oh, D. Y., Hofer, R. R., Katz, I., Sims, J. A., Warner, N. Z., Randolph, T. M., Reeve, R., and Moeller, R. C., "Benefits of Using Hall Thrusters for a Mars Sample Return Mission," *31st International Electric Propulsion Conference Proceedings, Ann Arbor, MI. September 20-24, 2009. IEPC-2009-217*.
- ⁶Hofer, R. R., Goebel, D. M., Snyder, J. S., and Sandler, I., "BPT-4000 Hall Thruster Extended Power Throttling Range Characterization for NASA Science Missions," *31st International Electric Propulsion Conference Proceedings Sept. 20-24, 2009, Ann Arbor, MI. IEPC-2009-085*.
- ⁷Hofer, R. R., "High-Specific Impulse Operation of the BPT-400 Hall Thruster for NASA Science Missions," *46th AIAA/ASME/SAE/ASEE Joint Propulsion Conference & Exhibit, July 25-28, 2010. Nashville, TN. AIAA-2010-6623*.
- ⁸De Grys, K., Mathers, A., and Welander, B., "Demonstration of 10,400 Hours of Operation on a 4.5 kW Qualification Model Hall Thruster," *46th Joint Propulsion Conference and Exhibit, July 25-28, 2010. Nashville, TN. AIAA-2010-6698*.
- ⁹Mikellides, I. G., Katz, I., Hofer, R. R., Goebel, D. M., de Grys, K., and Mathers, A., "Magnetic shielding of the channel walls in a Hall plasma accelerator," *Physics of Plasmas*, Vol. 18, No. 3, 2011, pp. 033501.
- ¹⁰Hoskins, W. A., Cassady, R. J., Morgan, O., Myers, R. M., Wilson, F., and King, D. Q., "30 Years of Electric Propulsion Flight Experience at Aerojet Rocketdyne," *33rd International Electric Propulsion Conference, Oct. 6-10, 2013. Washington, D.C. IEPC-2013-439*.
- ¹¹Fife, J., *Hybrid-PIC Modeling and Electrostatic Probe Survey of Hall Thrusters*, Ph.D Thesis, Massachusetts Institute of Technology, Cambridge, MA, 1999.
- ¹²Boeuf, J. P. and Garrigues, L., "Low frequency oscillations in a stationary plasma thruster," *Journal of Applied Physics*, Vol. 84, No. 7, 1998, pp. 3541–3554.
- ¹³Hagelaar, G. J. M., Bareilles, J., Garrigues, L., and Boeuf, J. P., "Two-dimensional model of a stationary plasma thruster," *Journal of Applied Physics*, Vol. 91, No. 9, 2002, pp. 5592–5598.
- ¹⁴Parra, F. I., Ahedo, E., Fife, J. M., and Martinez-Sanchez, M., "A two-dimensional hybrid model of the Hall thruster discharge," *Journal of Applied Physics*, Vol. 100, No. 2, 2006.
- ¹⁵Garrigues, L., Hagelaar, G. J. M., Boniface, C., and Boeuf, J. P., "Anomalous conductivity and secondary electron emission in Hall effect thrusters," *Journal of Applied Physics*, Vol. 100, No. 12, 2006.
- ¹⁶Sommier, E., Scharfe, M., Gascon, N., Cappelli, M., and Fernandez, E., "Simulating Plasma-Induced Hall Thruster Wall Erosion With a Two-Dimensional Hybrid Model," *Plasma Science, IEEE Transactions on*, Vol. 35, No. 5, Oct 2007, pp. 1379–1387.
- ¹⁷Hofer, R. R., Katz, I., Mikellides, I. G., Goebel, D. M., Jameson, K. K., Sullivan, R. M., and Johnson, L. K., "Efficacy of Electron Mobility Models in Hybrid-PIC Hall Thruster Simulations," *44th AIAA/ASME/SAE/ASEE Joint Propulsion Conference, July 21-23, 2008, Hartford, CT. AIAA-2008-4924*.
- ¹⁸Mikellides, I. G. and Katz, I., "Numerical simulations of Hall-effect plasma accelerators on a magnetic-field-aligned mesh," *Physical Review E*, Vol. 86, No. 4, Oct. 2012, pp. 046703.
- ¹⁹Bareilles, J., Hagelaar, G. J. M., Garrigues, L., Boniface, C., Boeuf, J. P., and Gascon, N., "Critical assessment of a two-dimensional hybrid Hall thruster model: Comparisons with experiments," *Physics of Plasmas*, Vol. 11, No. 6, 2004, pp. 3035–3046.
- ²⁰Mikellides, I., Katz, I., Hofer, R., and Goebel, D., "Design of a Laboratory Hall Thruster with Magnetically Shielded Channel Walls, Phase III: Comparison of Theory with Experiment," *48th AIAA/ASME/SAE/ASEE Joint Propulsion Conference & Exhibit, July 30- Aug 1, 2012. Atlanta, GA. AIAA-2012-3789*.
- ²¹De Grys, K., Welander, B., Dimicco, J., Wenzel, S., and Kay, B., "4.5 kW Hall Thruster System Qualification Status," *41st AIAA/ASME/SEA/ASEE Joint Propulsion Conference, July 10-13, 2005, Tuscon, AZ. AIAA-2005-3682*.
- ²²De Grys, K. H., Carpenter, C., Welander, B., Mathers, A., and Hofer, R. R., "Extended Duration Operation of BPT-4000 Qualification Unit at Low Power," *3rd JANNAF Spacecraft Propulsion Joint Subcommittee Meeting, Dec. 8-12, 2008, Orlando, FL*.
- ²³Welander, B. A. and De Grys, K. H., "Completion of the BPT-4000 Hall Thruster Qualification," *53rd JANNAF Propulsion Meeting, Dec. 5-8, 2005, Monterey, CA*.
- ²⁴Hofer, R., Goebel, D., Mikellides, I., and Katz, I., "Design of a Laboratory Hall Thruster with Magnetically Shielded Channel Walls, Phase II: Experiments," *48th AIAA/ASME/SAE/ASEE Joint Propulsion Conference & Exhibit, July 30- Aug 1, 2012. Atlanta, GA. AIAA-2012-3788*.
- ²⁵Staack, D., Raites, Y., and Fisch, N. J., "Shielded electrostatic probe for nonperturbing plasma measurements in Hall thrusters," *Review of Scientific Instruments*, Vol. 75, No. 2, 2004.
- ²⁶Chen, F. F., "Langmuir probe diagnostics," *Mini-Course on Plasma Diagnostics, IEEE-ICOPS Meeting, Jeju, Korea, 2003*.
- ²⁷Fruchtman, A., Zoler, D., and Makrinich, G., "Potential of an emissive cylindrical probe in plasma," *Phys. Rev. E*, Vol. 84, Aug 2011, pp. 025402.

²⁸Katz, I. and Goebel, D., *Fundamentals of Electric Propulsion: Ion and Hall Thrusters*, Vol. 1 of *JPL Space Science and Technology Series*, Wiley and Sons, 2008.

²⁹Mikellides, I. G., Katz, I., Hofer, R. R., and Goebel, D. M., "Magnetic shielding of a laboratory Hall thruster. I. Theory and validation," *Journal of Applied Physics*, Vol. 115, No. 4, Jan. 2014, pp. 043303.

³⁰Ortega, A. and Mikellides, I., "A New Cell-Centered Numerical Scheme for Ions in the 2-D Axisymmetric Code Hall2De," *50th AIAA/ASME/SAE/ASEE Joint Propulsion Conference and Exhibit, July 28-30, 2014, Cleveland, OH.*